Bicritical features of the metal-insulator transition in bandwidth-controlled manganites: Single crystals of $Pr_{1-x}(Ca_{1-y}Sr_y)_xMnO_3$

Y. Tomioka[1,2] and Y. Tokura[1,2,3]

[1]*Correlated Electron Research Center (CERC), National Institute of Advanced Industrial Science and Technology (AIST), Tsukuba 305-8562, Japan*

[2]*Joint Research Center for Atom Technology (JRCAT), National Institute of Advanced Industrial Science and Technology (AIST), Tsukuba 305-0046, Japan*

[3]*Department of Applied Physics, University of Tokyo, Tokyo 113-8656, Japan*

(Received 20 February 2002; published 16 September 2002)

The phase change from a charge- and orbital-ordered insulator to a ferromagnetic metal has been investigated for single crystals of $Pr_{0.55}(Ca_{1-y}Sr_y)_{0.45}MnO_3$ with controlled one-electron bandwidth. At $0 \leqslant y \leqslant 0.2$, the ground state is the charge- and orbital-ordered insulator, while for $y \geqslant 0.25$ it changes to a ferromagnetic metal. At around $y=0.25$, the critical temperatures for the charge-orbital ordering and the ferromagnetic transition coincide with each other ($\approx$200 K), forming the bicritical point in the electronic phase diagram. Around this insulator-metal phase boundary, prototypical colossal magnetoresistance emerges in the metallic regime, while the charge-orbital ordering is melted by a relatively low magnetic field of a few tesla in the charge- and orbital-ordered insulating regime. The phase diagrams of $Pr_{1-x}(Ca_{1-y}Sr_y)_xMnO_3$ ($0 \leqslant y \leqslant 1$) with various doping levels of $x=0.35$, 0.45, and 0.5 indicate that such a competition between the charge-orbital ordering and the ferromagnetic metal is critically dependent on the doping level. In particular, the commensurate doping level ($x=0.5$) tends to stabilize the charge- and orbital-ordered state even beyond the bicritical point in the lower-temperature side of the ferromagnetic phase.

DOI: 10.1103/PhysRevB.66.104416 PACS number(s): 75.30.Kz, 71.27.+a, 71.30.+h

I. INTRODUCTION

The manganese oxides with perovskite structure have extensively been investigated in recent years, which has revealed versatile intriguing phenomena including colossal magnetoresistance (CMR) due to a unique coupling among spin, charge, and orbital degrees of freedom of $3d$ electrons. In $R_{1-x}A_xMnO_3$, the chemical substitution of trivalent cations (R^{3+}) with the divalent ones (A^{2+}) produces a ferromagnetic metal, which has been attributed to the double-exchange (DE) mechanism.[1–5] Because of the ferromagnetic intra-atomic exchange between the e_g and t_{2g} electron spins (Hund's-rule coupling), the transfer interaction of the e_g electron between the neighboring Mn^{3+} ($3d^4;t_{2g}^3e_g^1$) and Mn^{4+} ($3d^3;t_{2g}^3e_g^0$) ions depends on the alignment of their local t_{2g} spin moments. With increase in the ferromagnetic alignment of the local t_{2g} spins, the transfer interaction increases or, equivalently, the ferromagnetic and metallic state is stabilized by the electron transfer. As recent theoretical studies[6,7] have indicated, the T_C of the DE ferromagnetism is to be scaled by the effective one-electron bandwidth of the e_g band (W).

From an experimental point of view, the W of $R_{1-x}A_xMnO_3$ is controlled by the averaged radius of R^{3+} and A^{2+} (Ref. 8). If the averaged radius decreases, the tilting of MnO_6 octahedra increases in an orthorhombically distorted structure. Then the hybridization between the manganese e_g and oxygen $2p$ states decreases or the W reduces. In the reduced-W cases, other interactions competing with the DE interaction become relatively important, such as the repulsive Coulomb interaction among the e_g electrons, the charge-orbital ordering (CO-OO),[9] the superexchange interaction between the local t_{2g} spins,[10,11] the collective Jahn-Teller distortion,[12,13] etc. In $Pr_{1-x}Ca_xMnO_3$ as the typical example of the reduced-W cases, the CO-OO is seen around $x=1/2$ ($0.3 \leqslant x < 0.75$).[14–16] At the transition temperature (T_{CO}), the compound undergoes the alternate ordering of Mn^{3+} and Mn^{4+} accompanied by the ordering of the e_g orbital on the Mn^{3+} sublattice in the orthorhombic ab plane of the $Pbnm$ lattice ($a_0 \times b_0 \times c_0 \approx \sqrt{2}a_p \times \sqrt{2}a_p \times 2a_p$, where a_p is the unit cell parameter of the pseudocubic lattice). With further decrease in temperature, the antiferromagnetic ordering [CE type at $x=0.5$ (Ref. 17) or the pseudo-CE type for $x \neq 0.5$ (Refs. 16 and 18)] sets in in the charge- and orbital-ordered state.

Upon the competition between the CO-OO and the metallic ferromagnetism, application of an external magnetic field energetically favors the latter, that is, the antiferromagnetic charge- and orbital-ordered insulator (CO-OOI) can be turned to the ferromagnetic metal (FM) by applying an external magnetic field.[19–22] In $Pr_{1-x}Ca_xMnO_3$, the stability of the CO-OO in magnetic fields depends on the deviation of x from 1/2.[23] The critical magnetic field for the melting of the CO-OO is as high as 27 T at $x=0.5$,[24] while it is lowered to a few tesla at $x=0.3$.[19] The change in the stability seems to be related with the x-dependent modification of the spin ordering along the c axis in the pseudo-CE type.[16,18] By utilizing the fragile CO-OO at $x=0.3$, many exotic ways of metal-insulator phase control have been demonstrated so far.[25–32]

In relation to the competition between the CO-OO and FM, a scenario of the electronic phase separation has recently been raised as a generic feature of the CMR systems.[33–35] In this model, a quenched disorder caused by the random chemical replacement at the perovskite A sites is

TABLE I. Lattice parameters (*Pbnm* setting), growth rates, analyzed cation ratios, and transition temperatures of $Pr_{1-x}(Ca_{1-y}Sr_y)_xMnO_3$ prepared by the floating zone method with the prescribed compositions $x=0.45$ and $y=0-1$.

y (nominal)	x $(Ca+Sr)/(Pr+Ca+Sr)$[a]	y $Sr/(Ca+Sr)$[a]	Lattice parameters a_0, b_0, c_0 [Å]	Growth rate [mm/h]	T_{CO}[b], T_C [K]
0	0.430	0	$a_0=5.4072$, $b_0=5.4258$, $c_0=7.6319$	2.2	[b]234
0.2	0.442	0.196	$a_0=5.4199$, $b_0=5.4203$, $c_0=7.6438$	2.2	[b]203
0.4	0.462	0.367	$a_0=5.4298$, $b_0=5.4180$, $c_0=7.6485$	2.2	226
0.6	0.433	0.594	$a_0=5.4511$, $b_0=5.4252$, $c_0=7.6554$	2.4	248
0.8	0.425	0.803	$a_0=5.4694$, $b_0=5.4323$, $c_0=7.6563$	3.5	275
1	0.431	1	$a_0=5.4830$, $b_0=5.4380$, $c_0=7.6534$	4	298

[a]The cation ratio was determined by the ICP (inductively coupled plasma) spectroscopy.
[b]The averaged value of the transition temperatures in the cooling and warming runs.

one of key factors to determine the sizes of the coexisting clusters of ferromagnetic and antiferromagnetic phases. Correspondingly, a metal-insulator transition due to chemical substitution, application of magnetic field, or decreasing temperature is supposed to occur in a percolative manner or via linking of the separated ferromagnetic clusters. However, most of the reported experimental data on the polycrystalline sintered specimens (ceramics) seem to be affected seriously by the presence of the grain boundaries possibly associated with the local strain effect more than by the random potential arising from the chemical substitution alone.

In this paper, we report the detailed study on the competition between the CO-OO and FM in the system of $Pr_{1-x}(Ca_{1-y}Sr_y)_xMnO_3$ ($0\leqslant y\leqslant 1$, $x=0.35$, 0.45, and 0.5) with use of single-crystal specimens. The systematic study was carried out on the melting of the CO-OO by a chemical substitution at the perovskite *A* site. Upon the substitution of Ca with Sr, while keeping the respective hole-doping level constant, the *W* increases, and the CO-OO is changed to the FM. At $x=0.45$, however, the competition is so crucial that the bicritical feature is pronounced in the vicinity of the insulator-metal phase boundary. Following the description of experimental procedures in Sec. II, we present an overview of the electronic phase diagrams of $Pr_{1-x}(Ca_{1-y}Sr_y)_xMnO_3$ ($0\leqslant y\leqslant 1$) with $x=0.35$, 0.45, and 0.5 in Sec. III. In Sec. IV, we concentrate on the multicritical features in $Pr_{1-x}(Ca_{1-y}Sr_y)_xMnO_3$ ($0\leqslant y\leqslant 1$) with $x=0.45$ crystals. The field-induced effects at $0\leqslant y\leqslant 0.2$ in relation with CO-OO features, an insulator-to-metal transition upon Sr substitution beyond $y=0.2$, and emergence of CMR near the insulator-metal phase boundary are described. A summary is given in Sec. V.

II. EXPERIMENTAL PROCEDURES

Single crystals of $Pr_{0.55}(Ca_{1-y}Sr_y)_{0.45}MnO_3$ were prepared by a floating zone method. The mixed powders of Pr_6O_{11}, $CaCO_3$, $SrCO_3$, and Mn_3O_4 with a prescribed ratio were calcined at 1050 °C for 12–24 h in air. The powders were pulverized and sintered again in the same condition. Then the powders were pressed into a rod with about 4 mm in diameter and 70 mm in length, and the rod was fired at 1200–1350 °C for 24 h in air. The sintering temperature was increased as the Sr concentration increases. The crystals were grown with use of a floating zone furnace equipped with double hemiellipsoidal mirrors coated with gold, in an oxygen atmosphere with rotating the feed and seed rods in opposite directions. The growth rate was changed from 2 to 4 mm/h with the Sr concentration. The obtained crystals were pulverized and checked by a powder x-ray diffraction (XRD) with Cu $K\alpha$ radiation. The XRD pattern was collected by the $\theta/2\theta$ step scanning method in the range of $15°\leqslant 2\theta\leqslant 110°$. Reitveld refinement of the XRD pattern indicated that the obtained crystal is a single phase. For $0\leqslant y\leqslant 0.8$, all the diffraction peaks were indexed by the orthorhombic *Pbnm* lattice while at $y=1$ those were by the orthorhombic *Imma*.[36] The analyzed cation ratio, the lattice parameters, the growth rate, and the magnetic transition temperatures of the obtained crystals are listed in Table I.

Magnetization was measured by a superconducting quantum interference device (SQUID) magnetometer (MPMS, Quantum Design Inc.). The electrodes for the resistivity measurement were made by a silver paste. Resistivity in magnetic fields was measured with use of the four-probe method in a cryostat equipped with a superconducting magnet up to 7 T.

III. OVERALL PHASE DIAGRAMS

Figure 1 shows the temperature profiles of resistivity of $Pr_{1-x}(Ca_{1-y}Sr_y)_xMnO_3$ ($0\leqslant y\leqslant 1$) single crystals with (a) $x=0.35$, (b) 0.45, and (c) 0.5, respectively. Let us first describe the cases of $x=0.35$ and 0.45. In Figs. 1(a) and 1(b), the CO-OO is seen at $0\leqslant y\leqslant 0.3$ and $0\leqslant y\leqslant 0.2$, respectively, which is manifested by a sudden increase in resistivity at around 220 K. The T_{CO} is systematically lowered as y increases. The CO-OO is, however, replaced by a FM for $y\geqslant 0.4$ and $y\geqslant 0.25$, respectively, and the T_C increases as y

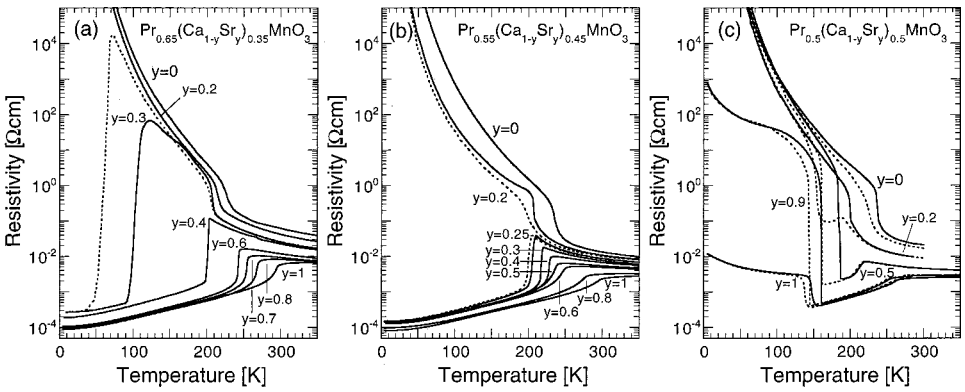

FIG. 1. Temperature profiles of resistivity for $Pr_{1-x}(Ca_{1-y}Sr_y)_xMnO_3$ ($0 \leqslant y \leqslant 1$) crystals with (a) $x=0.35$, (b) 0.45, and (c) 0.5. Solid and dotted lines denote the warming and cooling runs, respectively.

increases. Correspondingly, steep resistive transitions at T_C observed for $y=0.4$ and $y=0.25$ change to rather gradual ones at $y=1$. In the both cases of $x=0.35$ and 0.45, the features of the insulator-to-metal transition upon the substitution of Ca with Sr are quite similar although the critical y values for the transition are different. In Fig. 1(a), the resistivity for $y=0.3$ shows a large decrease (increase) around 70 K (100 K) in the cooling (warming) process.[37,38] Namely, at $y=0.3$, although the CO-OO once takes place at $\sim$200 K, it changes to a FM at lower temperatures. In Fig. 1(b), on the other hand, the resistivity of $y=0.2$ shows no sign of such a reentrant transition for $T<T_{CO}$.

In Fig. 1(c) for $x=0.5$, similarly to the aforementioned cases, the T_{CO} is lowered with increase in y. The FM phase emerges above $y=0.2$, and the T_C reaches 265 K at $y=1$.[39–42] However, the FM induced by the substitution of Ca with Sr undergoes the transition to the CO-OO at a lower temperature, which is typically seen at $y=0.5$ and 0.9. At $y=0.9$, the resistivity jump at $\sim$145 K in the cooling process is more than three orders of magnitude, comparable with the case of the CO-OO transition of $Nd_{0.5}Sr_{0.5}MnO_3$.[43] Thus the antiferromagnetic CE-type structure is perhaps kept up to $y=0.9$. At $y=1$, the resistivity at low temperatures is rather low in magnitude, and the antiferromagnetic (AF) structure is the A type as a former neutron diffraction study has proved.[40] According to a more recent study of neutron scattering,[44] a short-range stripe-type charge ordering exists in this A-type antiferromagnetic state.

Figure 2 shows the electronic phase diagrams of $Pr_{1-x}(Ca_{1-y}Sr_y)_xMnO_3$ ($0 \leqslant y \leqslant 1$) single crystals with (a) $x=0.35$, (b) 0.45, and (c) 0.5, respectively. In both cases of $x=0.35$ and 0.45, the antiferromagnetic CO-OOI is replaced by the FM with an increase in y, as shown in Figs. 2(a) and 2(b). In Fig. 2(a), however, the FM regime geometrically stretches out in the CO-OOI regime below $\sim$100 K at $y=0.3$. This gives rise to such a CO-OO reentrant transition as observed in the temperature dependence of resistivity for the $x=0.35$, $y=0.3$ crystal [Fig. 1(a)]. In Fig. 2(b) for $x=0.45$, on the other hand, the phase boundary between the CO-OOI and FM exists at $0.2<y<0.25$, i.e., within the $\Delta y<0.05$, and hence is almost parallel to the ordinate. As a result, the phase diagram for $x=0.45$ with respect to the CO-OOI and FM appears as a most prototypical example of the bicritical point feature.

In the case of $x=0.5$, as shown in Fig. 2(c), the CO-OOI is almost always dominant at low temperatures although the FM appears at a higher temperature at $y>0.2$. In other words, the CO-OOI regime widely stretches out in the FM regime below $\sim$170 K at $y>0.2$. In the low-temperature phase, the CE-type structure is kept at least up to $y=0.82$.[45] This corresponds to the FM–to–CO-OO transition with the decrease of temperature, as observed in Fig. 1(c). Note that the well-known FM–CO-OO transition in $Nd_{1/2}Sr_{1/2}MnO_3$ (Ref. 43) is also in this category. At $y=1$, the magnetic structure is turned into the A-type antiferromagnetic state, yet a stripe-type charge ordering exists.[44] In the case of $x=0.5$, the CO-OOI thus remains as the low-temperature phase even when the W is increased by the substitution of Ca with Sr. This is quite contrastive with the aforementioned cases of $x=0.35$ and 0.45. The stability of the CE-type CO-OO seems to be enhanced due to the commensurability of the doped

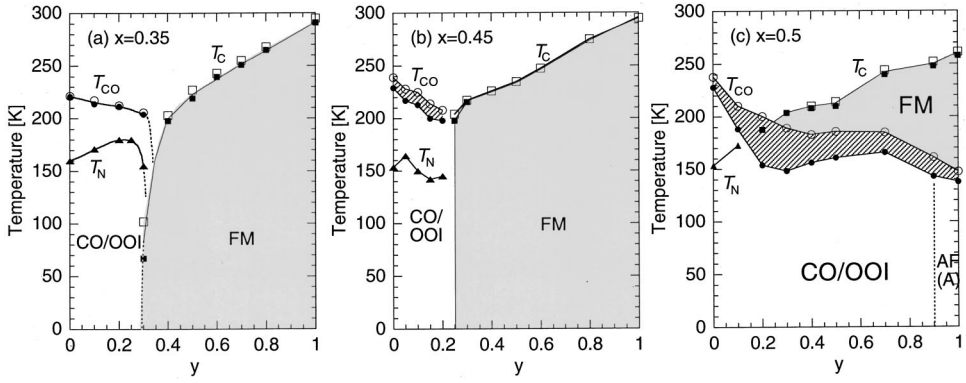

FIG. 2. Electronic phase diagrams of $Pr_{1-x}(Ca_{1-y}Sr_y)_xMnO_3$ ($0 \leqslant y \leqslant 1$) with (a) $x=0.35$, (b) 0.45, and (c) 0.5. The charge- and orbital-ordered insulator and ferromagnetic metal are denoted as CO-OOI and FM, respectively. The transition from (to) the CO-OOI is represented by open (solid) circles and that from (to) the FM by open (solid) squares, respectively. The Néel temperature T_N is indicated by solid triangles. The hysteresis region is hatched.

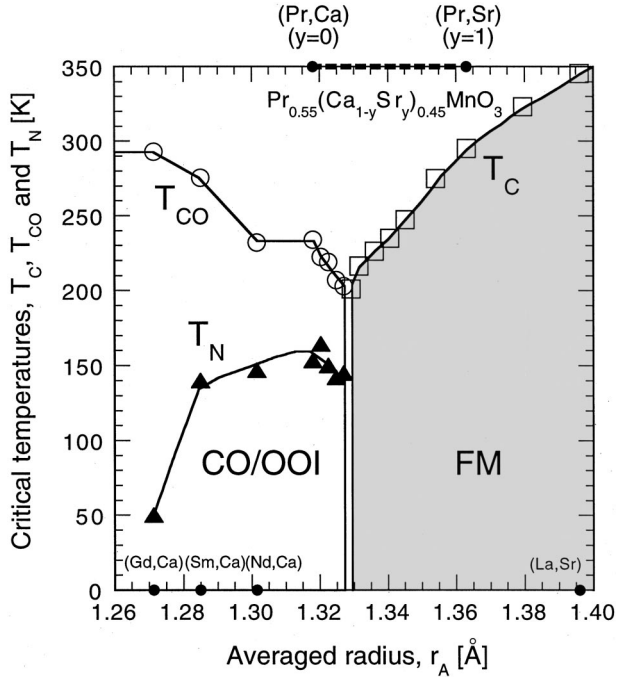

FIG. 3. Extended phase diagram for $x=0.45$ over a wide regime of the *A*-site-averaged ionic radius, which includes our own results for single crystals of $R_{1-x}Ca_xMnO_3$ ($x=0.45$, $R=$Gd, Sm, and Nd) as well as for $(Pr_{0.5}La_{0.5})_{1-x}Sr_xMnO_3$ and $La_{1-x}Sr_xMnO_3$ ($x=0.45$) in addition to those for the present $Pr_{1-x}(Ca_{1-y}Sr_y)_xMnO_3$ ($x=0.45$). The T_{CO} and T_C, which were determined by averaging the values in the cooling and warming runs, are indicated by open circles and squares, respectively. The antiferromagnetic charge- and orbital-ordered insulator and ferromagnetic metal are denoted as CO-OOI and FM, respectively. The Néel temperature T_N is denoted as solid triangles.

hole level. In what follows, we restrict ourselves to the bicritical features in the case of $x=0.45$.

IV. CRITICAL FEATURES IN $x=0.45$ CRYSTALS

First, we show in Fig. 3 the extended phase diagram for $x=0.45$ over a wide regime of the *A*-site-averaged ionic radius. To add the data points to the case of $Pr_{1-x}(Ca_{1-y}Sr_y)_xMnO_3$ ($x=0.45, 0\leqslant y\leqslant 1$), we have made use of our own results for single crystals of $R_{1-x}Ca_xMnO_3$ ($x=0.45$, $R=$Gd, Sm, and Nd) as well as for $(Pr_{0.5}La_{0.5})_{1-x}Sr_xMnO_3$ and $La_{1-x}Sr_xMnO_3$ ($x=0.45$). It is even more evident in this broader perspective that the competition between the CO-OO and FM exhibits the bi critical feature: Both T_{CO} and T_C systematically decrease toward the CO-OO–FM phase boundary and finally coincide with each other, $T_{CO}=T_C\approx 200$ K, forming the bicritical point. Incidentally, the AF spin ordering temperature T_N tends to decrease with decreasing the *A*-site ionic radius or the *W*, while showing a critical decrease only near the CO-OO–FM phase boundary. This reflects the fact that the CE-type spin ordering is mediated by the local double-exchange interaction along the orbital zigzag arrangement on the *ab* plane.[15–17]

Hereafter, coming back to the case of $Pr_{1-x}(Ca_{1-y}Sr_y)_xMnO_3$ ($x=0.45$), we investigate the step variation of magnetoresistive properties around the bicritical point. Figure 4 (left) shows the prototypical temperature profiles of magnetization (top), lattice parameters (middle), and resistivity (bottom) for the $y=0.05$ crystal of $Pr_{1-x}(Ca_{1-y}Sr_y)_xMnO_3$ ($x=0.45$) with the charge- and orbital-ordered ground state. As shown in the figure, the CO-OO transition at around 225 K($=T_{CO}$) is manifested by abrupt changes in magnetization, lattice parameters, and re-

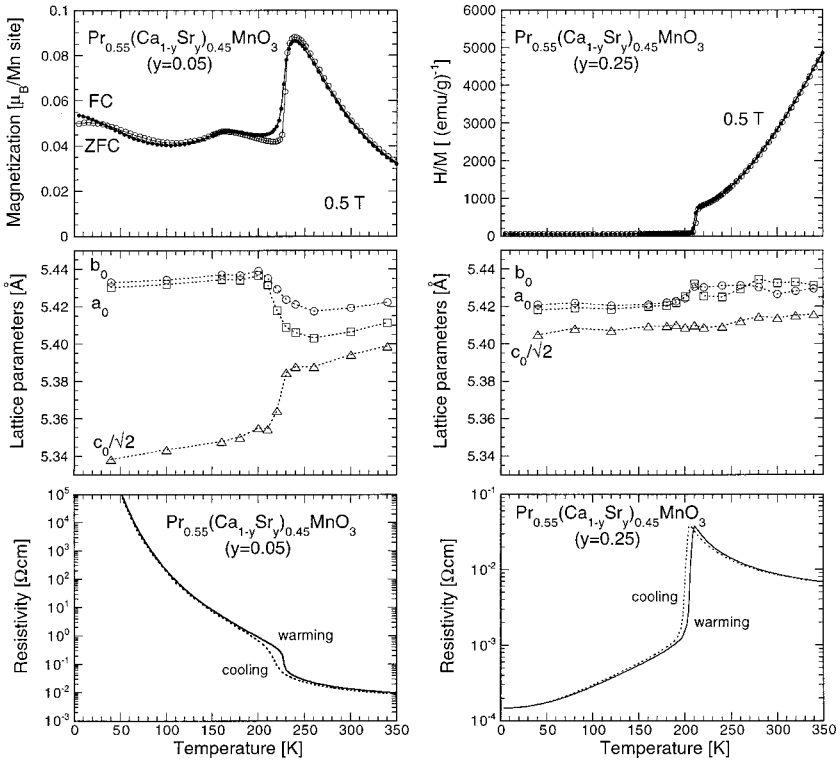

FIG. 4. Temperature profiles of magnetization (top), lattice parameters (middle), and resistivity (bottom) for $Pr_{0.55}(Ca_{1-y}Sr_y)_{0.45}MnO_3$ crystals with $y=0.05$ (left) and 0.25 (right). In the top panels, the zero-field cooling (ZFC) and field cooling (FC) magnetizations are denoted as open and solid circles, respectively. In the middle panels, the crystal axes are those of *Pbnm* symmetry. In the bottom panels, the cooling and warming runs are denoted as dotted and solid lines, respectively.

sistivity. Since the ferromagnetic fluctuation is mediated by the isotropic DE interaction, the onset of the CO-OO steeply suppresses the magnetization as observed. A cusp structure at ~160 K in the top panel of Fig. 4 (left) is perhaps due to the antiferromagnetic ordering. As shown in the middle panel of Fig. 4 (left), the *a* and *b* axes of the orthorhombic *Pbnm* cell elongate, while the *c* axis shrinks at T_{CO}. Such a uniaxial change of lattice parameters is generally seen upon the CO-OO transition of the perovskite manganites, e.g., in $Nd_{1/2}Sr_{1/2}MnO_3$ (Ref. 43), $La_{1/2}Ca_{1/2}MnO_3$ (Refs. 46 and 47), and $Nd_{1/2}Ca_{1/2}MnO_3$ (Ref. 48). The changes in lattice parameters are consistent with collective Jahn-Teller distortion arising from the e_g orbital ordering such as zigzag ordering of $d(3x^2-r^2)$ and $d(3y^2-r^2)$ orbitals on the *ab* plane.[15,16] Besides the change in lattice parameters, the superlattice diffractions due to the formation of the orbital superlattice appear below T_{CO} (Ref. 16).

Figure 4 (right) shows the temperature profiles of inverse susceptibility (top), lattice parameters (middle), and resistivity (bottom) for the $y=0.25$ crystal with the FM ground state. As shown in the top panel, the inversed susceptibility ceases decreasing near above T_C and shows a plateaulike feature and then abruptly drops at T_C, leading to the first-order transition to the ferromagnetic state. The observed features indicate that the antiferromagnetic interaction exists near above T_C, but is suddenly removed at T_C. This is occasionally seen in the reduced-*W* systems with $x\sim0.5$.[49,50] As seen in the middle panel, the lattice parameters a_0 and b_0 of the orthorhombic *Pbnm* cell tend to elongate as temperature approaches T_C, but suddenly shrink at T_C (Ref. 51). In the light of the collective Jahn-Teller effect, such a change in lattice parameters as observed in the middle panel indicates that the e_g orbital lying nearly within the *ab* plane immediately above T_C is turned to the randomly oriented or isotropic state below T_C (Refs. 9 and 51). This is just opposite to the change observed for $y=0.05$ at T_{CO}. In the bottom panel of Fig. 4 (right), a change in resistivity at T_C is shown to be larger than by one order in magnitude. All the results shown in Fig. 4 (right) indicate that an antiferromagnetic interaction exists near above T_C that is perhaps due to a CO-OO instability and that the antiferromagnetic interaction is suddenly removed at T_C. These features are quite generic for the CMR manganite, as has been typically observed in $Sm_{1-x}Sr_xMnO_3$ with the same doping level ($x=0.45$).[52] In the latter compound, in fact, it has been confirmed by the diffuse x-ray scattering as well as the Raman phonon scattering that the short-range CO-OO accompanied by collective Jahn-Teller distortion evolves down to T_C, but suddenly diminishes below T_C. Thus the critical competition between the CO-OO and FM is realized in the $y=0.25$ crystal on the verge of the insulator-metal phase boundary.

Figure 5 shows the temperature profiles of inversed susceptibility with varying *y* from 0 to 0.5. In accord with the temperature profiles of resistivity [Fig. 1(b)], the transition to the ferromagnetic state is seen for $y\geqslant0.25$. Another noteworthy aspect is that a deviation from the Curie-Weiss law is pronounced as *y* approaches the phase boundary. This means that near the bicritical point, i.e., $T_{CO}=T_C\sim200$ K and $y=0.25$, there is increasing competition between the CO-OO and FM and, hence, an increasing fluctuation of the respective components.

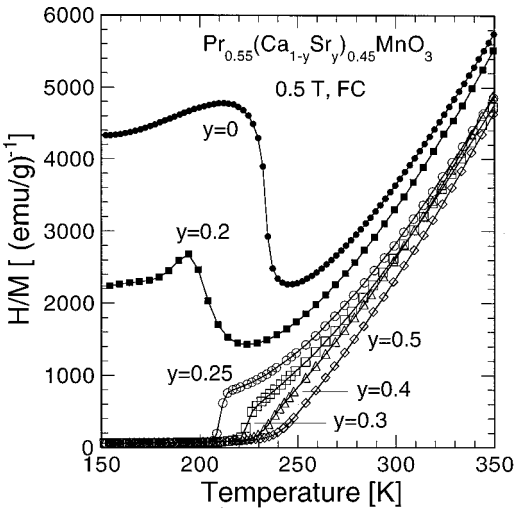

FIG. 5. Temperature profiles of inversed susceptibility for $Pr_{0.55}(Ca_{1-y}Sr_y)_{0.45}MnO_3$ crystals with varying *y* from 0 to 0.5. The magnetization was measured at 0.5 T.

The temperature profiles of resistivity in several magnetic fields of the $y=0.2$ and 0.25 crystals are shown in Fig. 6. In Fig. 6 (left), the resistivity curves at $\mu_0H\leqslant2$ T indicate the CO-OO transition at around 200 K and the subsequent insulating feature down to the lowest temperature. The resistivity for $\mu_0H\geqslant3$ T, on the other hand, shows no manifestation of the CO-OO, but a metallic feature below some critical temperature. The low-temperature phase below 200 K is abruptly switched as a whole from the CO-OOI to the FM by application of $\mu_0H=3$ T for this compound. In other words, the point of ($T_{CO}=T_C=200$ K, $\mu_0H=2-3$ T) also appears as the bicritical point in the (*T*,*H*) plane of the CO-OO phase diagram (see also the inset to Fig. 8). As the magnetic field is intensified, the metallic state is expanded to higher temperatures. A similar field-induced insulator-to-metal transition has been observed also for the $y=0.15$ crystal. In Fig. 6 (right) for $y=0.25$, however, a huge decrease in resistivity is already seen at zero field, and the resistive behavior in mag-

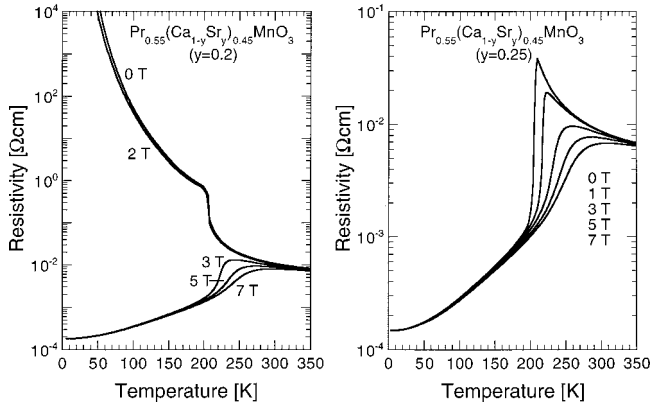

FIG. 6. Temperature profiles of resistivity in several magnetic fields for $Pr_{0.55}(Ca_{1-y}Sr_y)_{0.45}MnO_3$ crystals with $y=0.2$ (left) and 0.25 (right). These data were taken in the warming process.

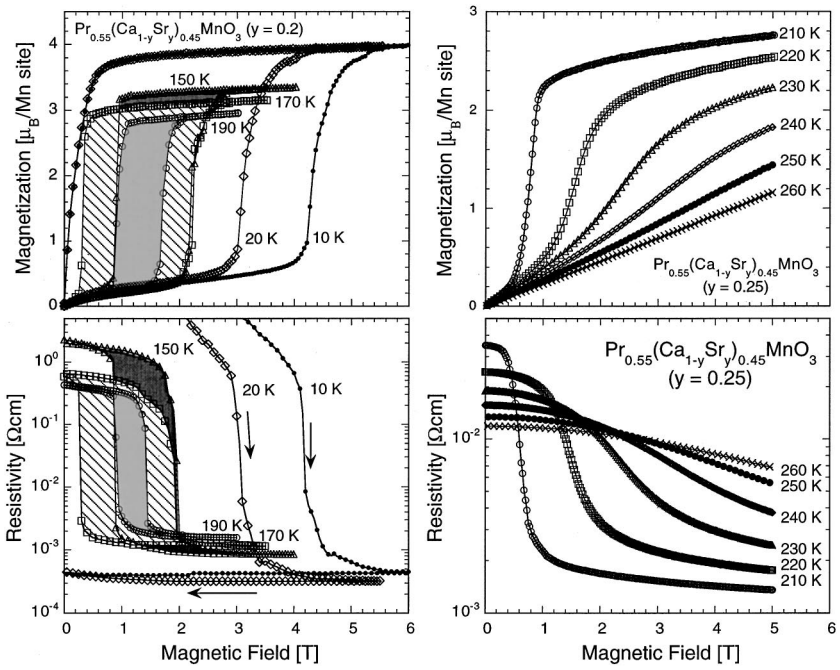

FIG. 7. Magnetization (upper) and resistivity (lower) isotherms for $Pr_{0.55}(Ca_{1-y}Sr_y)_{0.45}MnO_3$ crystals with $y=0.2$ (left) and 0.25 (right). The magnetization and resistivity isotherms were measured once the sample was cooled to a prescribed temperature in zero field. In the left panel, the bright, hatched, and dark regions are the hysteresis for $T=190$, 170, and 150 K, respectively. In the cases of $T=20$ and 10 K, the transitions are irreversible and the metallic state is kept even the magnetic field is removed.

netic fields shows the prototypical CMR feature. This again confirms that the competition between CO-OO and FM at $y=0.25$ is so critical that an application of an external magnetic field removes the antiferromagnetic correlation near above T_C and causes CMR

Figure 7 shows the magnetization (upper) and resistivity (lower) isotherms of the $y=0.2$ (left) and 0.25 (right) crystals. In the case of $y=0.2$, all the curves have been measured below T_{CO}, while in the case of $y=0.25$ those above T_C. In the upper panel of Fig. 7 (left), a metamagnetic transition is found to be accompanied by a hysteresis between the field increasing and decreasing runs. In the lower panel of Fig. 7 (left), the resistivity drop and jump are observed at corresponding metamagnetic transition fields. These features confirm that the antiferromagnetic CO-OOI is changed to the FM by application of magnetic field. On the basis of these isotherms with variation of an external magnetic field we have deduced the CO-OOI–FM phase diagram in the plane of temperature (T) and magnetic field (H), as shown in Fig. 8. The hatched region indicates the hysteresis between the field increasing and decreasing runs. As observed for other related manganites with the CE-type CO-OOI,[21–24,43] the hysteresis region is remarkablely expanded as the temperature is lowered. At 10 and 20 K, in particular, the field-induced *irreversible* CO-OOI–FM transitions show up in magnetoresistive behaviors [the lower panel of Fig. 7 (left)] as well as in the T-H phase diagram. This has been accounted for in terms of the supercooling or superheating effect in the course of the field-induced first-order phase transition between CO-OOI and FM.[19] As compared with the T-H phase diagrams in other systems, the critical magnetic field for the CO-OOI–FM transition is much reduced in the $y=0.2$ crystal. This is because the present $y=0.2$ crystal locates on the verge of the CO-OOI–FM phase boundary. A further noteworthy feature is that the lower critical field for the FM–CO-OOI transition once becomes small just above

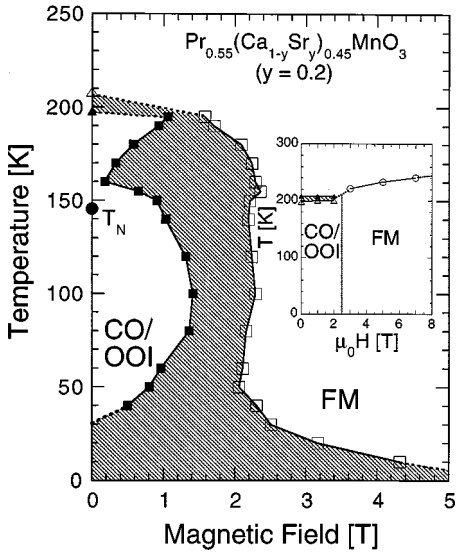

FIG. 8. Charge- and orbital-ordered insulator (CO-OOI) vs ferromagnetic metal (FM) phase diagram for a $Pr_{0.55}(Ca_{1-y}Sr_y)_{0.45}MnO_3$ crystal with $y=0.2$, which is demonstrated in the plane of temperature (T) and magnetic field (H). Open and solid squares indicate the critical fields from CO-OOI to FM and those from FM to CO-OOI, respectively, which were determined by the midpoint of the metamagnetic transition as shown in Fig. 7 (right). Open and solid triangles indicate T_{CO} at zero field, which were determined by the resistivity anomalies in the warming and cooling runs. The Néel temperature T_N is denoted as a solid circle. The hatched region indicates the hystresis between the field increasing and decreasing runs. The inset shows the similar CO-OOI–FM phase diagram determined by the thermal-scan resistivity measurements [Fig. 6 (left)] at constant magnetic fields. In the high-field region ($\mu_0 H \geq 3$ T), the temperatures of the inflection points of resistivity curves are tentatively shown by open circles as the crossover to the FM phase.

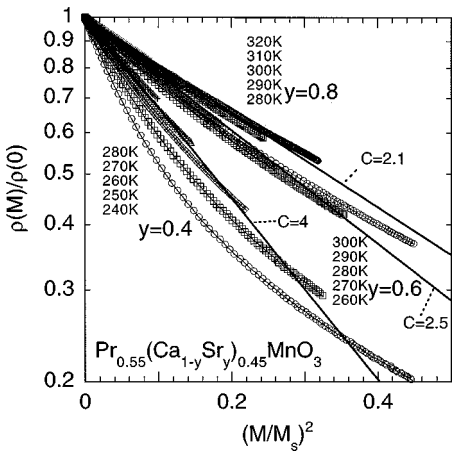

FIG. 9. Dependence of normalized resistivity as a function of the magnetization (M), $\rho(M)/\rho(0)$, for $Pr_{0.55}(Ca_{1-y}Sr_y)_{0.45}MnO_3$ crystals with $y=0.4$, 0.6, and 0.8. These curves were derived by combining the corresponding $M(H)$ and $\rho(H)$ data. The dotted lines represent the empirical relation that $\rho(M)/\rho(0)=\exp[-C(M/M_s)^2]$ (M_s being the saturation magnetization).

the CE-type spin ordering temperature T_N, but then increases with further lowering temperature (down to 100 K).[24] This reflects the fact that the CE-type long-range spin order works cooperately with the CO-OO to compete with the FM phase. Incidentally, the inset to Fig. 8 displays the phase diagram based on the thermal scan resistivity measurements at constant magnetic fields [Fig. 6 (left)].

In the upper panel of Fig. 7 (right), at temperatures just above T_C, e.g., at 210 K, the magnetization shows a steep increase at 0.5–1 T, in analogy to the metamagnetic transition. The feature indicates that an antiferromagneticlike state at zero field is changed to a ferromagnetic state by application of magnetic field. In accordance with the change in magnetization, the resistivity shows a large decrease at the corresponding magnetic field. Thus the removal of the antiferromagnetic correlation by application of an external magnetic field causes the CMR effect.[49–52] A similar feature is also visible for the crystals with $y=0.3$ and 0.4, although the field-induced changes in magnetization and resistivity become rather gradual with increase in y.

As y exceeds beyond 0.4, the magnitude of MR becomes smaller. Figure 9 shows the dependence of normalized resistivity on magnetization, $\rho(M)/\rho(0)$, for several crystals with $y\geqslant 0.4$. These curves are derived by combining the corresponding $M(H)$ and $\rho(H)$ data. In the figure, the $\rho(M)/\rho(0)$ is approximated by an empirical formula that $\rho(M)/\rho(0)=\exp[-C(M/M_s)^2]$ (M_s being a saturation magnetization).[53–55] In the simple DE model, the MR is interpreted as due to the decrease in spin scattering of the e_g orbital carriers. The dynamical mean field theory[6,7] predicts that in the low-M ($\ll M_s$) region the coefficient C varies from unity in the weak-coupling limit ($J_H/W\sim 1$) to 4 in the strong-coupling regime ($J_H/W\gg 1$) (J_H being the energy of Hund's-rule coupling). In Fig. 9, the $\rho(M)/\rho(0)$ at $y=0.4$ is quite temperature dependent, and it is not well fitted even by the empirical formula as temperature approaches T_C. The coefficient C in the low-M limit is obviously larger than 4 near T_C. At $y=0.6$ and 0.8, on the other hand, the temperature variation of $\rho(M)/\rho(0)$ is rather convergent and can be fitted by the formula with the coefficient C smaller than 4. Therefore, the CMR behavior at $0.25\leqslant y\leqslant 0.4$, whose origin is ascribed to the field suppression of the charge-orbital correlation as well as of the associated antiferromagnetic spin correlation, changes to the conventional MR due to a field-induced decrease in spin scattering for $y>0.4$ with the increased W.

V. SUMMARY

In single crystals of $Pr_{0.55}(Ca_{1-y}Sr_y)_{0.45}MnO_3$ with controlled one-electron bandwidth, we have investigated the phase change from the charge-orbital ordering to the ferromagnetic metal. At $0\leqslant y\leqslant 0.2$, the ground state is the charge- and orbital-ordered insulator, while for $y\geqslant 0.25$ it changes to a ferromagnetic metal. Around the phase boundary, the notable decreases in both T_{CO} and T_C are seen until the both transition temperatures meet to coincide with each other, forming the bicritical point ($y=0.25$ and $T_{CO}=T_C\sim 200$ K). Near this bicritical point, the prototypical CMR feature shows up in the ferromagnetic metallic side, whereas the melting of the charge-orbital ordering by relatively low magnetic fields of a few tesla is observed in the charge- and orbital-ordered insulating side. It is found that the competition between the charge-orbital ordering and the ferromagnetic metal is dependent on the doping level. The commensurability of the hole concentration with the charge-orbital ordering is of importance to determine the phase diagram of $Pr_{1-x}(Ca_{1-y}Sr_y)_xMnO_3$. In particular, at $x=0.5$, the charge- and orbital-ordered state with the CE-type spin order is robust and extends to the lower-temperature region below the ferromagnetic metallic phase up to $y=0.9$.

ACKNOWLEDGMENTS

The authors would like to thank N. Nagaosa and E. Dagotto for helpful discussions. This work partly supported by NEDO (New Energy and Industrial Technology Development Organization) of Japan was performed under the joint research agreement between the ATP (Angstrom Technology Partnership) and NAIR (National Institute for Advanced Interdisciplinary Research).

[1] G. H. Jonker and J. H. van Santen, Physica (Amsterdam) **16**, 337 (1950).
[2] G. H. Jonker, Physica (Amsterdam) **22**, 707 (1956).
[3] C. Zener, Phys. Rev. **82**, 403 (1951).
[4] P. W. Anderson and H. Hasegawa, Phys. Rev. **100**, 675 (1955).
[5] P.-G. de Gennes, Phys. Rev. **118**, 141 (1960).
[6] N. Furukawa, J. Phys. Soc. Jpn. **64**, 2734 (1995).
[7] N. Furukawa, J. Phys. Soc. Jpn. **64**, 2754 (1995).

[8] J. B. Torrance, P. Laccore, A. I. Nazzal, E. J. Ansaldo, and Ch. Niedermayer, Phys. Rev. B **45**, 8209 (1992).
[9] Y. Tokura and N. Nagaosa, Science **288**, 462 (2000).
[10] R. Maezono, S. Ishihara, and N. Nagaosa, Phys. Rev. B **57**, R13 993 (1998).
[11] R. Maezono, S. Ishihara, and N. Nagaosa, Phys. Rev. B **58**, 11 583 (1998).
[12] A. J. Millis, P. B. Littlewood, and B. I. Shraiman, Phys. Rev. Lett. **74**, 5144 (1995).
[13] A. J. Millis, R. Mueller, and B. I. Shraiman, Phys. Rev. B **54**, 5405 (1996).
[14] E. Pollert, S. Krupicka, and E. Kuzmicova, J. Phys. Chem. Solids **43**, 1137 (1982).
[15] Z. Jirak, S. Krupicka, V. Nekvasil, E. Pollert, G. Villeneuve, and F. Zounova, J. Magn. Magn. Mater. **15–18**, 519 (1980).
[16] Z. Jirak, S. Krupicka, Z. Simsa, M. Dlouha, and Z. Vratislav, J. Magn. Magn. Mater. **53**, 153 (1985).
[17] E. O. Wollan and W. C. Koehler, Phys. Rev. **100**, 545 (1955).
[18] H. Yoshizawa, H. Kawano, Y. Tomioka, and Y. Tokura, Phys. Rev. B **52**, R13 145 (1995).
[19] Y. Tomioka, A. Asamitsu, Y. Moritomo, and Y. Tokura, J. Phys. Soc. Jpn. **63**, 1689 (1995).
[20] M. R. Lees, J. Barratt, G. Balakrishnan, D. McK. Paul, and M. Yethiraj, Phys. Rev. B **52**, R14 303 (1995).
[21] G. Xiao, E. J. McNiff, G. O. Gong, A. Gupta, C. L. Canedy, and J. Z. Sun, Phys. Rev. B **54**, 6073 (1996).
[22] K. Liu, X. W. Wu, K. H. Ahn, T. Sulchek, C. L. Chien, and J. Q. Xiao, Phys. Rev. B **54**, 3007 (1996).
[23] Y. Tomioka, A. Asamitsu, H. Kuwahara, Y. Moritomo, and Y. Tokura, Phys. Rev. B **53**, R1689 (1996).
[24] M. Tokunaga, N. Miura, Y. Tomioka, and Y. Tokura, Phys. Rev. B **57**, 5259 (1998).
[25] V. Kiryukhin, D. Casa, J. P. Hill, B. Keimer, A. Vigliante, Y. Tomioka, and Y. Tokura, Nature (London) **386**, 813 (1997).
[26] K. Miyano, T. Tanaka, Y. Tomioka, and Y. Tokura, Phys. Rev. Lett. **78**, 4257 (1997).
[27] A. Asamitsu, Y. Tomioka, H. Kuwahara, and Y. Tokura, Nature (London) **388**, 50 (1997).
[28] N. A. Babushkina, L. M. Belova, D. I. Khomskii, K. I. Kugel, O. Yu. Gorbenko, and A. R. Kaul, Phys. Rev. B **59**, 6994 (1999).
[29] S. Srivastava, N. K. Pandey, P. Padhan, and R. C. Budhani, Phys. Rev. B **62**, 13 868 (2000).
[30] A. Guha, N. Khare, A. K. Raychaudhuri, and C. N. R. Rao, Phys. Rev. B **62**, R11 941 (2000).
[31] H. Y. Hwang, S-W. Cheong, P. G. Radaelli, M. Marezio, and B. Batlogg, Phys. Rev. Lett. **75**, 914 (1995).
[32] A. Maignan, Ch. Simon, V. Caignaert, and B. Raveau, J. Magn. Magn. Mater. **152**, L5 (1996).
[33] A. Moreo, M. Mayr, A. Feiguin, S. Yunoki, and E. Dagotto, Phys. Rev. Lett. **84**, 5568 (2000).
[34] M. Uehara, S. Mori, C. H. Chen, and S.-W. Cheong, Nature (London) **399**, 560 (1999).
[35] J. Burgy, M. Mayr, V. Martin-Mayor, A. Moreo, and E. Dagotto, Phys. Rev. Lett. **87**, 277202 (2001).
[36] V. Caignaert, F. Millange, M. Hervieu, E. Suard, and B. Raveau, Solid State Commun. **99**, 173 (1996).
[37] Y. Tomioka, A. Asamitsu, H. Kuwahara, Y. Moritomo, and Y. Tokura, J. Phys. Soc. Jpn. **66**, 302 (1997).
[38] H. Yoshizawa, R. Kajimoto, H. Kawano, Y. Tomioka, and Y. Tokura, Phys. Rev. B **55**, 2729 (1997).
[39] Y. Tomioka, A. Asamitsu, Y. Moritomo, H. Kuwahara, and Y. Tokura, Phys. Rev. Lett. **74**, 5108 (1995).
[40] H. Kawano, R. Kajimoto, H. Yoshizawa, Y. Tomioka, H. Kuwahara, and Y. Tokura, Phys. Rev. Lett. **78**, 4253 (1997).
[41] D. N. Argyriou, D. G. Hinks, J. F. Mitchell, C. D. Potter, A. J. Shultz, D. M. Young, J. D. Jorgensen, and S. D. Bader, J. Solid State Chem. **124**, 381 (1996).
[42] F. Damay, C. Martin, M. Hervieu, A. Maignan, B. Raveau, and G. Andre, J. Magn. Magn. Mater. **184**, 71 (1998).
[43] H. Kuwahara, Y. Tomioka, A. Asamitsu, Y. Moritomo, and Y. Tokura, Science **270**, 961 (1995).
[44] R. Kajimoto, H. Yoshizawa, Y. Tomioka, and Y. Tokura (unpublished).
[45] Z. Jirak, F. Damay, M. Herview, C. Martin, B. Raveau, G. Andre, and F. Bouree, Phys. Rev. B **61**, 1181 (2000).
[46] P. G. Radaelli, D. E. Cox, M. Marezio, S.-W. Cheong, P. E. Schiffer, and A. P. Ramirez, Phys. Rev. Lett. **75**, 4488 (1995).
[47] P. G. Radaelli, D. E. Cox, M. Marezio, and S.-W. Cheong, Phys. Rev. B **55**, 3015 (1997).
[48] T. Vogt, A. K. Cheetham, R. Mahendiran, A. K. Raychaudhuri, R. Mahesh, and C. N. R. Rao, Phys. Rev. B **54**, 15 304 (1996).
[49] H. Kuwahara, Y. Tomioka, Y. Moritomo, A. Asamitsu, M. Kasai, R. Kumai, and Y. Tokura, Science **272**, 80 (1996).
[50] H. Kuwahara, Y. Moritomo, Y. Tomioka, A. Asamitsu, M. Kasai, and Y. Tokura, J. Appl. Phys. **81**, 4954 (1997).
[51] H. Kuwahara, Y. Moritomo, Y. Tomioka, A. Asamitsu, M. Kasai, R. Kumai, and Y. Tokura, Phys. Rev. B **56**, 9386 (1997).
[52] Y. Tomioka, H. Kuwahara, A. Asamitsu, M. Kasai, and Y. Tokura, Appl. Phys. Lett. **70**, 3609 (1997).
[53] S. von Molnar and S. Methfessel, J. Appl. Phys. **38**, 959 (1967).
[54] N. G. Bebenin and V. V. Ustinov, J. Phys.: Condens. Matter **10**, 6301 (1998).
[55] Y. Tomioka, A. Asamitsu, and Y. Tokura, Phys. Rev. B **63**, 024421 (2000).